



Cite this: *Environ. Sci.: Nano*, 2015, 2, 288

## Supercritical CO<sub>2</sub>-philic nanoparticles suitable for determining the viability of carbon sequestration in shale

Yisheng Xu,<sup>†ab</sup> Lin Chen,<sup>†bc</sup> Yushi Zhao,<sup>d</sup> Lawrence M. Cathles<sup>\*d</sup> and Christopher K. Ober<sup>\*b</sup>

Received 7th January 2015,  
Accepted 14th March 2015

DOI: 10.1039/c5en00003c

rsc.li/es-nano

A fracture spacing less than a decimeter is probably required for the successful sequestration of CO<sub>2</sub> in shale. Tracer experiments using inert nanoparticles could determine if a fracturing this intense has been achieved. Here we describe the synthesis of supercritical CO<sub>2</sub>-philic nanoparticles suitable for this application. The nanoparticles are ~50 nm in diameter and consist of iron oxide (Fe<sub>3</sub>O<sub>4</sub>) and silica (SiO<sub>2</sub>) cores functionalized with a fluorescent polymeric corona. The nanoparticles stably disperse in supercritical carbon dioxide (scCO<sub>2</sub>) and are detectable to concentrations of 10 ppm.

### Nano impact

Nanoparticles can be used to evaluate the uniformity of supercritical CO<sub>2</sub> sequestration in shale which is the most abundant and safest storage medium. For storage the shale must be fractured, and to pass through these fractures the nanoparticles must be <50 nm in diameter. They must also be stable at the reservoir temperatures of 60 °C and detectable to ppm concentrations. This paper documents the development of <50 nm nanoparticles with SiO<sub>2</sub> and Fe<sub>3</sub>O<sub>4</sub> cores that are functionalized with a fluorescent polymeric corona, disperse stably in supercritical CO<sub>2</sub>, and are detectable to 10 ppm.

## Introduction

Supercritical carbon dioxide (scCO<sub>2</sub>) has been applied to enhanced gas recovery (EGR) for more than 30 years,<sup>1</sup> and has recently found application in enhanced coal bed methane (ECBM) production.<sup>2</sup> Other applications range from caffeine extraction to semiconductor processing.<sup>3,4</sup> Sequestration of carbon dioxide in depleted gas shale reservoirs has been suggested as a way to remediate “green house” gas emissions.<sup>5</sup> One aspect, which is of great importance in enhanced hydrocarbon recovery or scCO<sub>2</sub> sequestration is the ability of the supercritical CO<sub>2</sub> to diffuse from the fractures through which it is introduced into the surrounding matrix which contains large volumes of pore space filled with stagnant methane. The distribution of flow fractures (fracture which transmit flow) in shales is almost completely unknown. One might measure it in the drill core and perhaps at the well

bore, but how the pattern of flow changes away from the well (where it counts for storage), is essentially unknown.

Dual tracer tests provide a way of measuring the uniformity of fracture flow and the effectiveness of diffusional exchange with the matrix.<sup>6</sup> The concept is that nanoparticles will travel through the fractures in the scCO<sub>2</sub> and diffuse very little into the surrounding pore space whereas chemical tracers will diffuse rapidly enough into this pore space to explore the total porosity. If nanoparticles together with a chemical tracer are passed between two wells, the early arrival of the particles compared to the chemical could directly measure how much of the pore space might be eventually filled with scCO<sub>2</sub>.<sup>7</sup>

A prerequisite for the implementation of dual tracer methods for scCO<sub>2</sub> sequestration are nanoparticles of appropriate size, dispersible in scCO<sub>2</sub> and detectable at ppm concentrations. We seek nanoparticles of ~50 nm diameter that will have diffusion constants 1.5 to 2 orders of magnitude greater than chemical tracers in scCO<sub>2</sub>. The main design criteria for the particles in this work are that they are small enough to pass through pore channels through which flow is occurring (which particles <50 nm will satisfy), that they form stable dispersions in scCO<sub>2</sub> up to temperatures of at least 60 °C (the temperature of likely shale sequestration strata), and that they are inert and do not become trapped

<sup>a</sup> State Key Laboratory of Chemical Engineering, East China University of Science and Technology, Shanghai 200237, China

<sup>b</sup> Materials Science and Engineering, Cornell University, Ithaca, NY 14853, USA. E-mail: christopher.ober@cornell.edu

<sup>c</sup> Chemistry and Chemical Biology, Cornell University, Ithaca, NY 14853, USA

<sup>d</sup> Earth and Atmospheric Sciences, Cornell University, Ithaca, NY 14853, USA. E-mail: lmc19@cornell.edu

<sup>†</sup> These authors contributed equally to this work.

(not stick) on rock minerals. This paper describes the preparation of nanoparticles needed to implement the dual tracer tests in shale, as illustrated in Fig. 1.

There exist very few examples of prior related work.<sup>8</sup> Very few studies have focused on the preparation of  $\text{scCO}_2$  dispersible NPs even though some reports have focused on polymer synthesis in  $\text{scCO}_2$ .<sup>9,10</sup> Cooper reported  $\text{scCO}_2$  soluble fluorinated polymeric dendrimers to extract hydrophilic compounds from water but did not use a hard core nanoparticle.<sup>11</sup> Grignard *et al.*<sup>12</sup> developed a method to prepare  $\text{CO}_2$ -soluble catalyst from silica supported fluorinated polymers by supercritical fluid extraction, but the fact that large particles could be easily centrifuged out of solution indicates poor solubility of the materials in  $\text{scCO}_2$ .

In this paper, we describe a simple and broadly applicable method to transform inorganic oxide NP cores into  $\text{scCO}_2$ -philic nanoparticles. This new hybrid particle class is composed of an inorganic core with a corona of fluorinated polymer chains, which are covalently bonded to the core through a surface-initiated atom transfer radical polymerization (SI-ATRP) reaction.<sup>13–17</sup> The NP cores (*e.g.* 7 nm (diameter) silica and 10 nm (diameter) iron oxide NPs) are well dispersed throughout the entire modification process. The polymer grafting density on two different inorganic cores was compared based on the solubility in  $\text{scCO}_2$ . The as-synthesized nanoparticles exhibit good dispersion properties even at diameters less than 50 nm in either  $\text{scCO}_2$  or in hydrofluoroether (HFE). HFE, due to its similarity to  $\text{scCO}_2$  such as low viscosity, low surface tension, and compatibility with fluoropolymer, *etc.* was used as a simple-to-handle analogue of  $\text{scCO}_2$  for characterization under ambient pressure, room temperature conditions.<sup>18</sup> Incorporation of a fluorescent label in the polymer corona has been shown to enable good detectability of the nanoparticles, to provide extra functionality in  $\text{scCO}_2$  tracer applications.

The novel aspect of this work is the development of nanoparticles for a specific tracer application (evaluating the feasibility of  $\text{CO}_2$  sequestration in shale). Successful preparation was not straight forward. Successful dispersion required increasing the time interval of polymer attachment in the synthesis process. The iron core of one of the particles synthesized allows SEM imaging of both the particle core and coronae. But mainly the procedures documented are important for the specific application of  $\text{CO}_2$  sequestration.

## Experimental section

### Materials and methods

Ferrous sulfate heptahydrate ( $\text{FeSO}_4 \cdot 7\text{H}_2\text{O}$ ), ferric chloride hexahydrate ( $\text{FeCl}_3 \cdot 6\text{H}_2\text{O}$ ), oleic acid (OA), (3-aminopropyl) trimethoxysilane,  $\alpha$ -bromoisobutyryl bromide, copper(I) bromide,  $N,N,N',N'',N'''$ -pentamethyldiethylenetriamine (PMDETA) (99%), 3,3,4,4,5,5,6,6,7,7,8,8,9,9,10,10-heptadecafluorodecyl methacrylate (97%), triethylamine (TEA), toluene anhydrous (99.8%) and Ludox SM30 silica NP were purchased from Sigma Aldrich. 1-Pyrenylmethyl methacrylate was purchased from Polysciences. Ethoxy-nonafluorobutane (HFE 7200) was purchased from 3M. Heptadecafluorodecyl methacrylate was passed through an alumina column to remove inhibitor. 1-Pyrenylmethyl methacrylate dissolved in THF was passed through a silica column to remove inhibitor. All other solvents and reagents were used as received without further purification.

### Synthesis of 2-bromo-2-methyl- $N$ -(3-(trimethoxysilyl)propyl)propanamide (BMTP)

$\alpha$ -Bromoisobutyryl bromide (6.72 mL, 0.053 mol) dissolved in 20 mL methylene chloride was added dropwise into a mixture of (3-aminopropyl) trimethoxysilane (12 mL, 0.067 mol) and TEA (13.96 mL, 0.1 mol) and 60 mL methylene chloride at 0 °C and the reaction was kept at room temperature. After 4 hour reaction, white precipitate was removed by vacuum filtration. The filtrate was washed with HCl (pH 2–3), brine and distilled water respectively and dried over anhydrous magnesium sulfate. The final product was obtained as colorless liquid after rotary vaporization (9.30 g, yield = 53.2%). <sup>1</sup>H NMR (300 MHz,  $\text{CDCl}_3$ ):  $\delta$  = 3.58 (s, 9H,  $-\text{Si}-\text{O}-\text{CH}_3$ ), 3.26 (t, 2H,  $-\text{CH}_2-\text{NH}-$ ), 1.96 (s, 6H,  $-\text{CH}_3$ ), 1.65 (m, 2H,  $-\text{CH}_2-\text{CH}_2-\text{CH}_2-$ ), 0.67 (t, 2H,  $-\text{Si}-\text{CH}_2-$ ).

### Synthesis of monodispersed $\text{Fe}_3\text{O}_4$ -NPs

The synthetic procedure was followed by the method described by Sun *et al.*<sup>19</sup> 2.35 g  $\text{FeSO}_4 \cdot 7\text{H}_2\text{O}$  and 4.1 g  $\text{FeCl}_3 \cdot 6\text{H}_2\text{O}$  were dissolved into 100 mL distilled water in a 250 mL flask. Iron oxide NPs were prepared by quickly adding 25 mL 27% (w/w) ammonium hydroxide under vigorous stirring at room temperature. 1 mL OA was then dropped into the formed black NP precipitate at 80 °C for 1 hour. The above reactions were carried out under nitrogen atmosphere. This OA functionalized

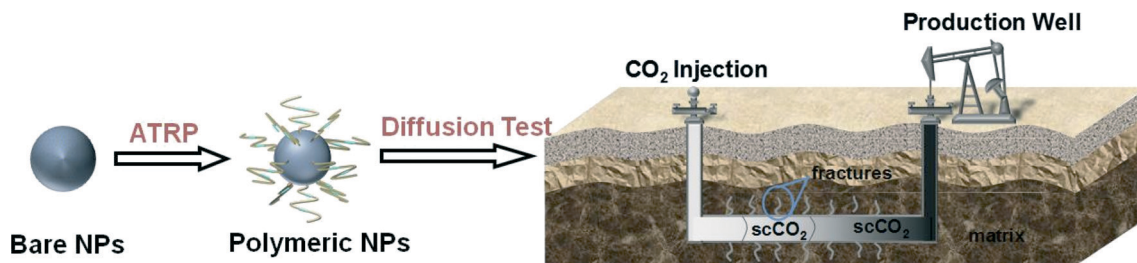


Fig. 1 NP tracer structure.  $\text{Fe}_3\text{O}_4$  and  $\text{SiO}_2$  NP cores were functionalized with  $\text{scCO}_2$ -philic polymeric corona for application in field-tests to estimate diffusion matrix storage.

NPs were then extracted with 25 mL toluene twice in the presence of small amount of sodium chloride in order to disperse the NP into organic solvent. To obtain a higher concentration of NPs, less toluene should be used in extraction. Finally, the NP dispersion was dried over anhydrous sodium sulfate and the concentration of the NP dispersion was determined to be 15 mg mL<sup>-1</sup>. Such NPs were shown to be magnetic since they can be separated under magnetic fields.

#### Preparation of initiator modified Fe<sub>3</sub>O<sub>4</sub>-NPs

BMTP (1.19 g), 20 mL 2 M TEA in toluene and 30 mL NPs were mixed together into a round flask. The mixture was allowed to react under nitrogen for 24 hours. After reaction, 20 mL petroleum ether was added to precipitate the NPs followed by magnetic separation of NPs. The NPs then were redispersed in 15 mL toluene. Such a process was repeated 3 times to remove the unreacted BMTP and remaining OA. The NPs were finally vacuum dried and ready for polymerization. TGA analysis shows the initiator immobilized on Fe<sub>3</sub>O<sub>4</sub> is ~22% (w/w) of total mass.

#### Surface polymerization on initiator modified Fe<sub>3</sub>O<sub>4</sub>-NPs

10 mg of initiator modified Fe<sub>3</sub>O<sub>4</sub>-NP were dissolved with cosolvents of DMF and TFT (50:50 v/v) in a Schlenk flask followed by 30 minutes purge with argon. In another flask, CuBr (4.7 mg, 0.03 mmol), PMDETA (8 μL, 0.038 mmol), heptadecafluorodecyl methacrylate (0.67 mL, 2 mmol), and 1-pyrenylmethyl methacrylate (20 mg, 0.07 mmol) were dissolved in 3 mL cosolvent of DMF and TFT (50:50 v/v). The mixture was freeze-thawed three times to remove oxygen. The mixture was then transferred into the NP solution under argon atmosphere and the reaction was carried out at 70 °C for 7 hours. The resulted precipitate polymer functionalized NPs were collected through vacuum filtration. To remove the CuBr residue, the solid was sonicated and then stirred in methanol overnight and the polymer modified NP powder was collected by filtration with CuBr retained in the filtrate.

#### Preparation of initiator modified SiO<sub>2</sub>-NPs

Ludox SM 30 particles instead of solid state fumed silica NPs were first passed through a cation exchange resin to protonate the NP solution. The choice of stable dispersed Ludox NPs is to avoid large aggregates when fumed silica was used. The solution was then dialyzed against DMF by using a cellulose membrane (MW cutoff: 7 K) for 48 hours with 1 change of DMF. The SiO<sub>2</sub> NPs were precipitated by HFE followed by centrifugation and the product was dried. The concentration of such NP solution was determined to be 115 mg mL<sup>-1</sup>. 1 mL of SiO<sub>2</sub> dispersion in DMF was further diluted in 9 mL DMF followed by addition of 11.45 g initiator. The solution was stirred at room temperature for 24 hours. The excess initiator was removed by dialysis against DMF for 96 hours with 4 changes of DMF. The content of SiO<sub>2</sub> was finally determined to be 8 mg mL<sup>-1</sup> by the same precipitation method

described above. TGA analysis shows the initiator immobilized on SiO<sub>2</sub> is ~25% (w/w) of total mass.

#### Surface polymerization on initiator modified SiO<sub>2</sub>-NPs

1 mL of initiator modified SiO<sub>2</sub>-NP solution was added in a Schlenk flask followed by 30 minutes purge with argon. In another flask, CuBr (5.7 mg, 0.04 mmol), PMDETA (10 μL, 0.048 mmol), heptadecafluorodecyl methacrylate (0.59 mL, 1.8 mmol), and 1-pyrenylmethyl methacrylate (10 mg, 0.035 mmol) were dissolved in 3 mL DMF. The mixture was freeze-thawed three times to remove oxygen. The mixture was then transferred into the NP solution under argon atmosphere and the reaction was carried out at 70 °C for 7 hours. The resulting polymer functionalized NP precipitate was collected through vacuum filtration. To remove the CuBr residue, the solid was stirred in methanol overnight and the polymer modified NP powder was collected.

#### Characterizations

DLS was carried out at 25 °C with a Malvern Zetasizer Nano ZS instrument equipped with a temperature control and using a 633 nm He-Ne laser for backscattering at 173°. The measurement duration was 15 seconds, and 11 measurements were averaged for each analysis. The distributions of the mean apparent translational diffusion coefficients ( $D_T$ ) were determined by fitting the DLS autocorrelation functions using nonnegative constrained least squares (NNLS). The distribution of apparent sizes  $D_h$  was obtained from the distribution of mean apparent translational diffusion coefficients ( $D_T$ ) via

$$D_h = kT/(6\pi\eta D_T) \quad (1)$$

where  $k$  is the Boltzmann constant, and  $\eta$  is the solvent viscosity which was assumed to be that of HFE. NP samples were dissolved in HFE and sonicated for 5 minutes followed by filtering with 0.2 μm filter. Gel permeation chromatography was performed by using a HLC-8220 GPC equipped with a TOSOH PL mixed-CX2 column and refractive index detector. Asahi KLIN AK225 (SEC grade) was used as the eluent at a flow rate of 1 mL min<sup>-1</sup> at 37 °C. Poly(methyl methacrylate) was used as a calibration standard. TEM was performed with a LEO 1550 FESEM under TEM mode at 30 kV and SEM images were taken at 5 kV with the same instrument. The sample was prepared by pipetting a drop of NP solution onto a carbon-coated Cu grid and dried in the air. Thermogravimetric analysis (TGA) was carried out using an Exstar TG/DTA6000. An amount of 3–7 mg of sample was used at a heating rate of 10 °C min<sup>-1</sup> from room temperature to 600 °C. Attenuated total reflection infrared spectroscopy (ATR-IR) was recorded on a Thermo Nicolet (iZ10) spectrometer. The dried powder sample was placed on a Ge crystal and the atmosphere background was subtracted by using OMNIC software. UV and fluorescence spectra were measured using a SpectraMax M2e in HFE. The excitation wavelength 340 nm

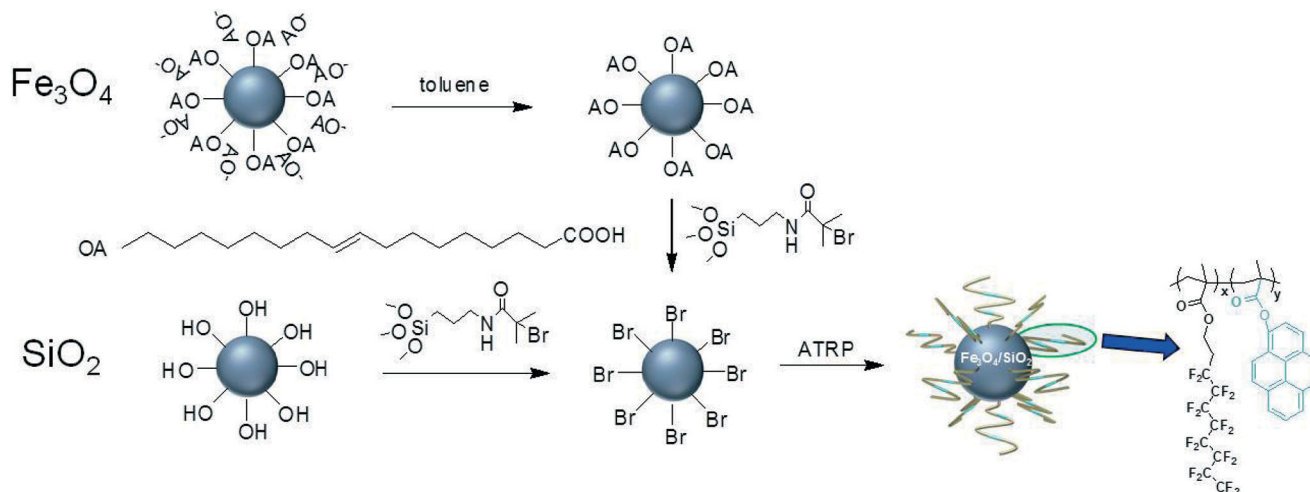


Fig. 2 Synthetic scheme of fluorescent fluorinated polymer functionalized nanoparticles.

was used for fluorescence measurements. Finally,  $\text{scCO}_2$  solubility tests were performed in a supercritical fluid phase monitor (SFT-phase monitor II) equipped with a 30 mL cell in which 20 mg of NPs were tested under different temperature and pressure conditions.

## Results and discussion

### Preparation of fluoropolymer functionalized $\text{Fe}_3\text{O}_4$ -NPs and $\text{SiO}_2$ -NPs

Initiator ( $\alpha$ -bromoisobutyryl bromide) functionalized iron oxide NPs were prepared through a ligand exchange method as reported by Sun *et al.*<sup>19</sup> As shown in Fig. 2, stable monodispersed NPs were first prepared by co-precipitation in the presence of OA. After extraction with toluene, the monodispersed NPs were stabilized by exposing hydrophobic alkyl moieties in toluene. Initiator was then covalently functionalized on the NPs by displacement of OA.<sup>19</sup> After precipitation and redispersion of the NPs with petroleum ether and toluene respectively, unattached initiator molecules were removed and the NPs were dried under vacuum.<sup>19</sup> Such NPs can be well dispersed in DMF for further ATRP reaction with addition of both fluorinated and fluorescent monomers. In the polymerization step, DMF was originally used as the solvent for ATRP since the monomers are soluble while the polymer is insoluble. As expected, the resulting product precipitated after polymerization. However, the  $\text{Fe}_3\text{O}_4$  NPs prepared in DMF are not completely soluble in HFE and  $\text{scCO}_2$  and a mixed solvent medium of DMF and TFT was used as discussed later in the section of effects of TFT on the solubility of  $\text{Fe}_3\text{O}_4$ -NPs. The polymerization on the  $\text{SiO}_2$ -NP surface was performed by using the same method. The molecular weights and polydispersity of the attached polymer determined by GPC were given in Table 1. However, the silica NPs are much more liable to aggregate and it is difficult to redisperse them due to strong H-bonding between particles especially at low pH conditions.<sup>20</sup> Therefore the monodispersed state of the silica particle needs to be maintained throughout all modification procedures. In

Table 1 GPC results of polymer ligands. Polymers were obtained by ATRP of pure initiator at the same conditions at which polymerization on NPs was performed

	$M_n$	$M_w$	$M_w/M_n$
Polymer ( $\text{Fe}_3\text{O}_4$ )	23 000	29 000	1.315
Polymer ( $\text{SiO}_2$ )	22 000	29 000	1.294

order to achieve monodispersed NPs, Ludox particles in aqueous solution were initially solvent exchanged with DMF instead of starting with solid state fumed silica NPs. After attaching the initiator onto the NPs, the excess initiator was removed by intensive dialysis against DMF.

### Characterizations of polymerized $\text{Fe}_3\text{O}_4$ -NPs and $\text{SiO}_2$ -NPs

DLS was used to monitor the size distributions of NPs at different synthetic steps as shown in Fig. 3a–c. OA, initiator, and polymer functionalized NPs can all be dispersed well in corresponding solvents with hydrodynamic diameters of 9, 10, and 43 nm respectively. In general, very little aggregation or cluster formation was observed from DLS during each reaction step. The final polymer-functionalized NPs were stable in solution for over a month as monitored by DLS. The DLS results are consistent with TEM analysis as indicated in Fig. 4a and b. Due to the low contrast of the polymeric corona, only the  $\text{Fe}_3\text{O}_4$  core can be observed by TEM. Large agglomerated patches were seen (Fig. 4a) but the NPs were more dispersed after polymer functionalization (Fig. 4b). Similar behavior could be found for silica NPs before (Fig. 4c) and after (Fig. 4d) polymerization. In addition, the spacing between two NPs suggests the existence of polymer coronas on  $\text{SiO}_2$ -NPs which is in contrast to the closely packed structure for bare NPs. Furthermore, SEM images of  $\text{Fe}_3\text{O}_4$  NPs before (Fig. 5a) and after (Fig. 5b) polymerization support the successful functionalization of polymer on NPs. As can be seen in the SEM images, from the shaded corona around the white solid spheres and their size, analysis of the NPs is

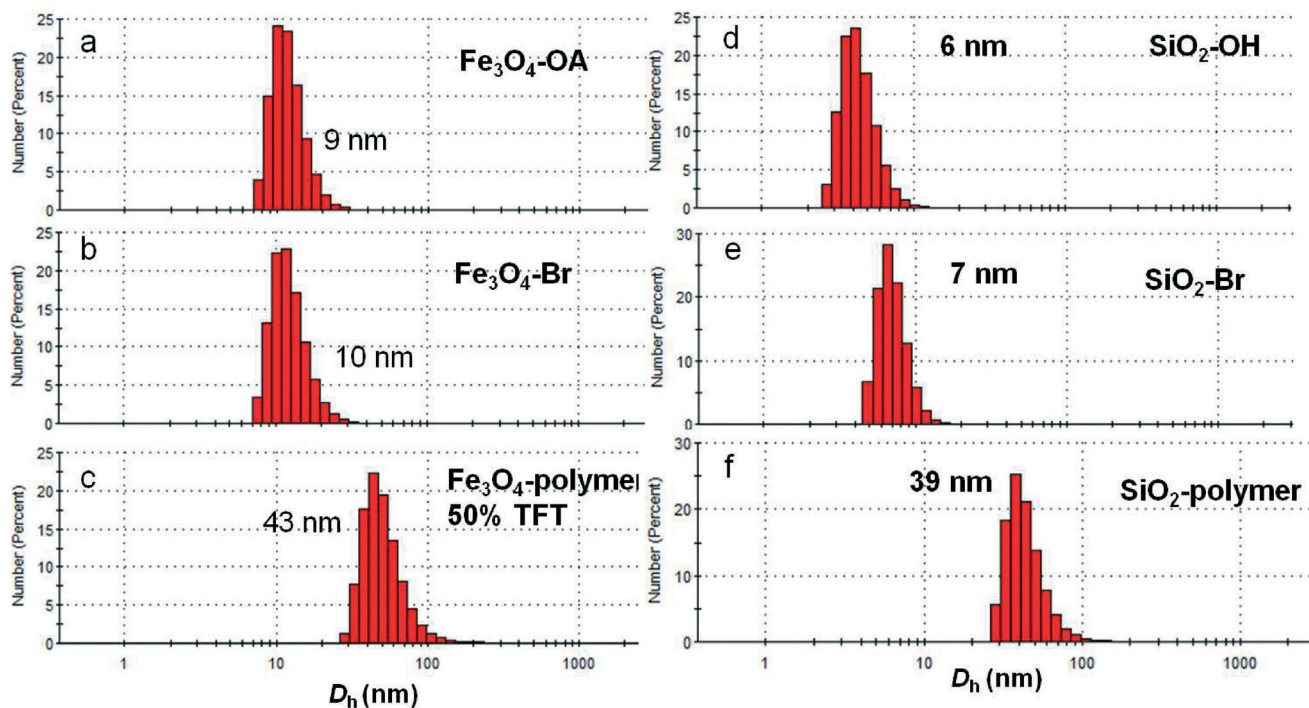


Fig. 3 Hydrodynamic diameter distributions of (a) OA coated  $\text{Fe}_3\text{O}_4$  in toluene; (b) initiator modified  $\text{Fe}_3\text{O}_4$ -NP in DMF; (c) fluoropolymer functionalized  $\text{Fe}_3\text{O}_4$ -NP in HFE; (d) bare Ludox silica in basic water; (e) initiator modified  $\text{SiO}_2$ -NP in DMF; (f) fluoropolymer functionalized  $\text{SiO}_2$ -NP in HFE.

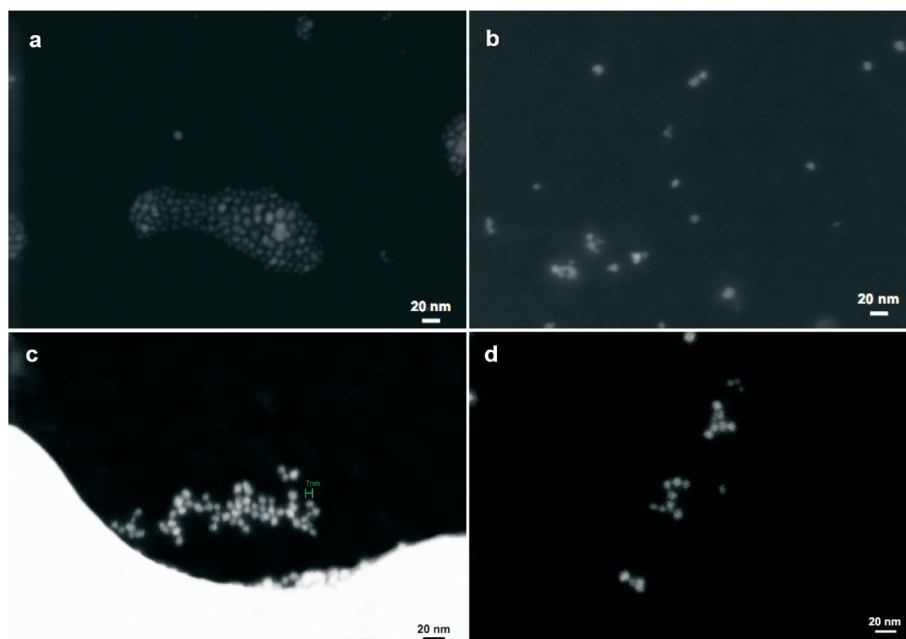


Fig. 4 TEM of (a) initiator coated  $\text{Fe}_3\text{O}_4$  NPs; (b) polymer functionalized  $\text{Fe}_3\text{O}_4$  NPs; (c) bare  $\text{SiO}_2$  NPs; (d) polymer functionalized  $\text{SiO}_2$  NPs.

generally consistent with that determined by DLS. In some cases, the size including the hard sphere and shaded polymer coating is larger than the DLS results probably because of the agglomeration of NPs in the SEM sample preparation step.

IR spectroscopy was then used to assess the functionalization process of iron oxide as presented in Fig. 6a. The stretching

modes of the alkyl moieties of OA were clearly seen between  $2800$  and  $3000\text{ cm}^{-1}$  and the carboxylate group of OA could be seen at  $1701\text{ cm}^{-1}$ .<sup>19</sup> After ligand exchange, amide I and II peaks were observed at  $1645$  and  $1534\text{ cm}^{-1}$  respectively indicating successful attachment of initiator.<sup>21</sup> The disappearance of high frequency stretching peaks between

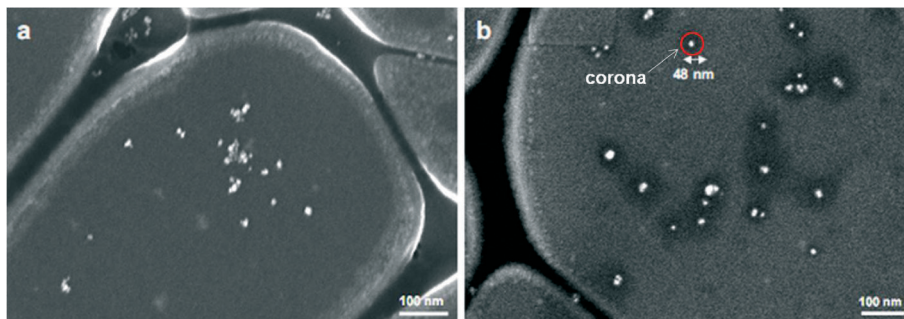


Fig. 5 SEM of (a) initiator coated  $\text{Fe}_3\text{O}_4$  NPs; (b) polymer functionalized  $\text{Fe}_3\text{O}_4$  NPs.

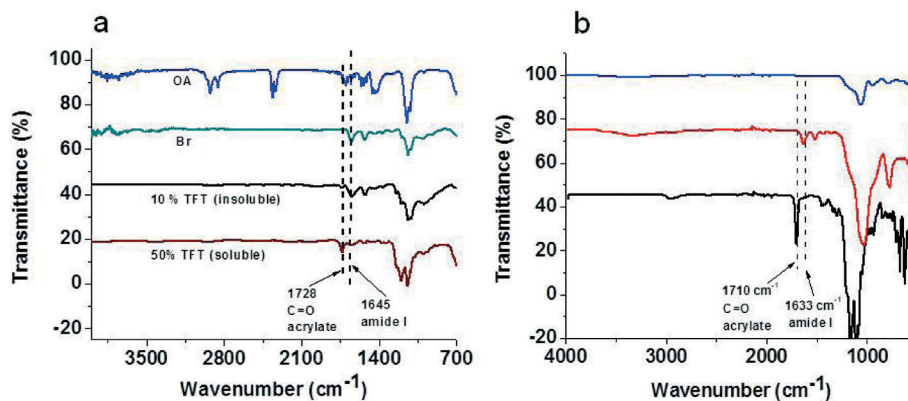


Fig. 6 IR characterization of  $\text{Fe}_3\text{O}_4$ -NP (a) and  $\text{SiO}_2$ -NP (b) modification at different process steps.

2800–3000  $\text{cm}^{-1}$  and the carboxylate peak at 1701  $\text{cm}^{-1}$  further suggests the complete ligand exchange without OA molecules remaining on the NPs. When polymerization took place in TFT/DMF = 1:9 solvent mixture, very little carbonyl stretching at 1728  $\text{cm}^{-1}$  was observed and the entire spectrum was very similar to that for initiator NPs.<sup>22</sup> However, increasing the TFT/DMF ratio from 0.1 to 1 dramatically increased the 1728  $\text{cm}^{-1}$  peak indicating large amount of polymer brushes were grown on the NP surface. The modifications of initiator and polymer on silica NPs monitored by IR are quite similar to those for  $\text{Fe}_3\text{O}_4$ -NP functionalization as shown in Fig. 6b.

TGA was also performed to determine the grafting density of initiator coated NPs (Fig. 7). Since the mass loss for

initiator-NP is about 25% of the total mass of Br-NP, the content of the initiator on NP is about 1.06  $\text{mmol g}^{-1}$ . The grafting density of initiator can be estimated by the following equation as reported by Liu *et al.*<sup>21</sup>

$$\text{GD} = \frac{a_{\text{Br}} N_{\text{A}}}{\frac{S}{\rho V}} \quad (2)$$

where GD is grafting density,  $a_{\text{Br}}$  is mole of initiator per gram of NP,  $N_{\text{A}}$  is Avogadro's number,  $S$  is the surface area of NP,  $V$  is the volume of NP, and  $\rho$  is the density of NP. Therefore, the grafting density of initiator can be estimated to be 5 initiators per  $\text{nm}^2$  for  $\text{Fe}_3\text{O}_4$ -NP and 2 initiators per  $\text{nm}^2$  for

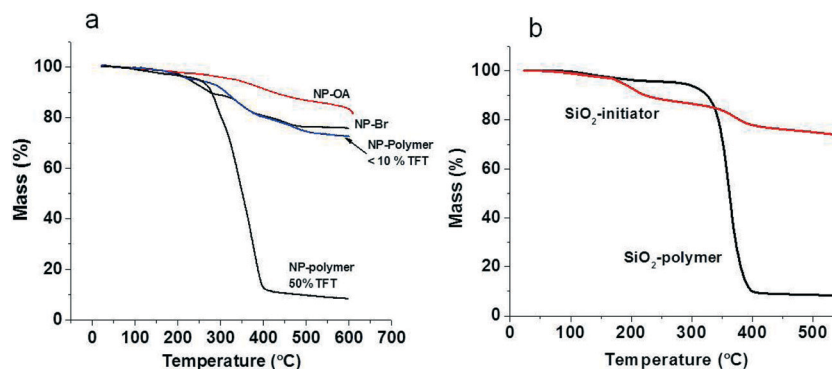


Fig. 7 TGA analysis of  $\text{Fe}_3\text{O}_4$ -NPs (a) and  $\text{SiO}_2$ -NPs (b) modifications at different steps.

SiO<sub>2</sub>-NP as shown in Table 2. By using the same calculations, the grafting density for fluoropolymer on Fe<sub>3</sub>O<sub>4</sub> and SiO<sub>2</sub> NPs are 0.15 and 0.056 polymers nm<sup>-2</sup>.

### Effect of TFT on Fe<sub>3</sub>O<sub>4</sub>-NPs solubility

The iron oxide NPs polymerized in pure DMF are not soluble in either HFE or scCO<sub>2</sub>. Sediment was observed after several minutes. This is probably because of the limited amount of polymer grafted on the surface due to fast precipitation in DMF, which therefore makes NPs poorly dispersible. One strategy to resolve this insolubility issue was to add selected amounts of trifluorotoulene (TFT) which extended the polymerization time before polymer precipitated from the solution. Adding only 10% (v/v) of TFT as cosolvent in DMF did not make the NPs soluble in HFE/scCO<sub>2</sub>. Infrared spectroscopy in Fig. 6a shows that very little polymerization took place on the NPs since the carbonyl peak at 1728 cm<sup>-1</sup> from the fluorinated monomer is negligible. This conclusion was further supported by TGA experiments, showing that

polymerized NPs have a very similar mass loss ratio to that of initiator modified NPs, which suggests little polymerization on NPs. Increasing the TFT volume ratio to 50% led to successful dissolution of the resulting NPs in HFE/scCO<sub>2</sub> with an observed hydrodynamic diameter of 43 nm. Further IR results suggest a significant increase in the peak ratio of acrylate carbonyl peak over amide I peak of initiator. TGA data also shows 90% mass loss at 600 °C attributed to the loss of attached polymer.

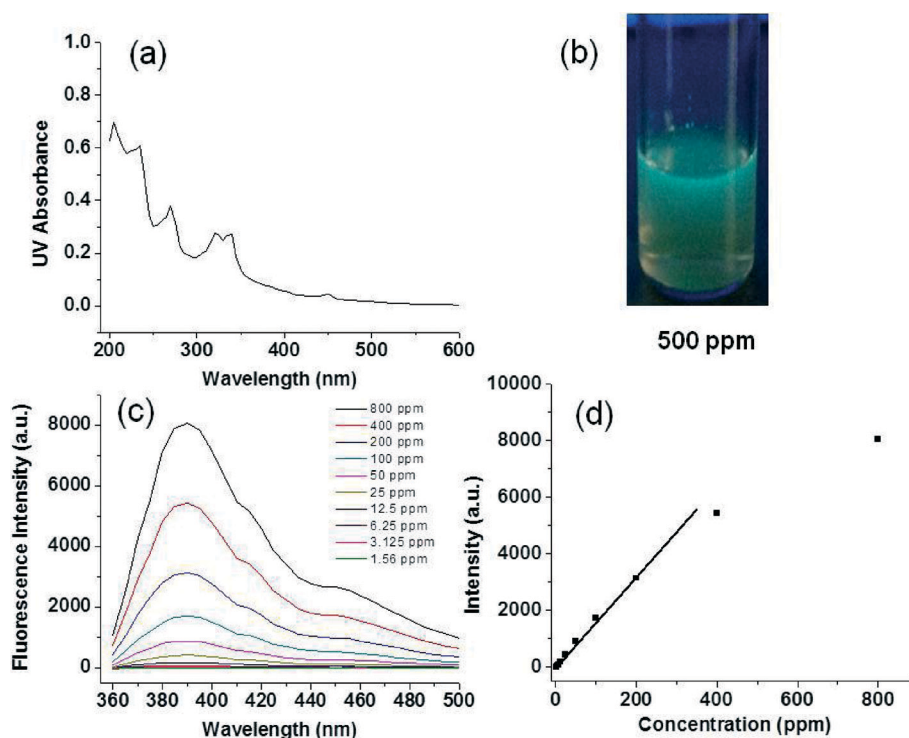
### UV absorbance and fluorescence properties of Fe<sub>3</sub>O<sub>4</sub>-NPs and SiO<sub>2</sub>-NPs

Fig. 8a shows a UV spectrum of Fe<sub>3</sub>O<sub>4</sub>-NP when 3.5% (mol) fluorescent monomer, 1-pyrenylmethyl methacrylate, was incorporated in the polymerization process. The peak at 340 nm corresponds to the characteristic peak of 1-pyrenylmethyl methacrylate and the elevated baseline arises from the absorption by the Fe<sub>3</sub>O<sub>4</sub> core.<sup>23</sup> Such NPs show very intense fluorescence (Fig. 8b and c). As seen in Fig. 8d

**Table 2** Parameters used in the estimation of the grafting density

	w% of ligand	$M_w$ (g mol <sup>-1</sup> )	$a_{Br}^a$ (mmol g <sup>-1</sup> )	$\rho$ (g cm <sup>-3</sup> )	$r$ (nm)	$S$ (nm <sup>2</sup> )	$V$ (nm <sup>3</sup> )	GD (#/nm <sup>2</sup> )
Fe <sub>3</sub> O <sub>4</sub> -initiator	0.25	235	1.06	5.00	5.00	314.2	523.6	5
SiO <sub>2</sub> -initiator	0.25	235	1.06	2.65	3.50	153.9	179.6	2
Fe <sub>3</sub> O <sub>4</sub> -polymer	0.662	23 000	2.88	5.00	5.00	314.2	523.6	0.15
SiO <sub>2</sub> -polymer	0.666	23 000	3.02	2.65	3.50	153.9	179.6	0.056

<sup>a</sup>  $M_n$  of polymer obtained from Table 1 was used to calculate  $a_{Br}$ .



**Fig. 8** (a) UV-vis spectrum of polymer functionalized Fe<sub>3</sub>O<sub>4</sub>-NPs; (b) Fe<sub>3</sub>O<sub>4</sub> NPs solution under UV excitation; (c) fluorescence spectra of Fe<sub>3</sub>O<sub>4</sub> NPs at a series of concentrations; (d) fluorescence calibration curve of Fe<sub>3</sub>O<sub>4</sub>-NPs. HFE was used in all spectroscopic analysis.

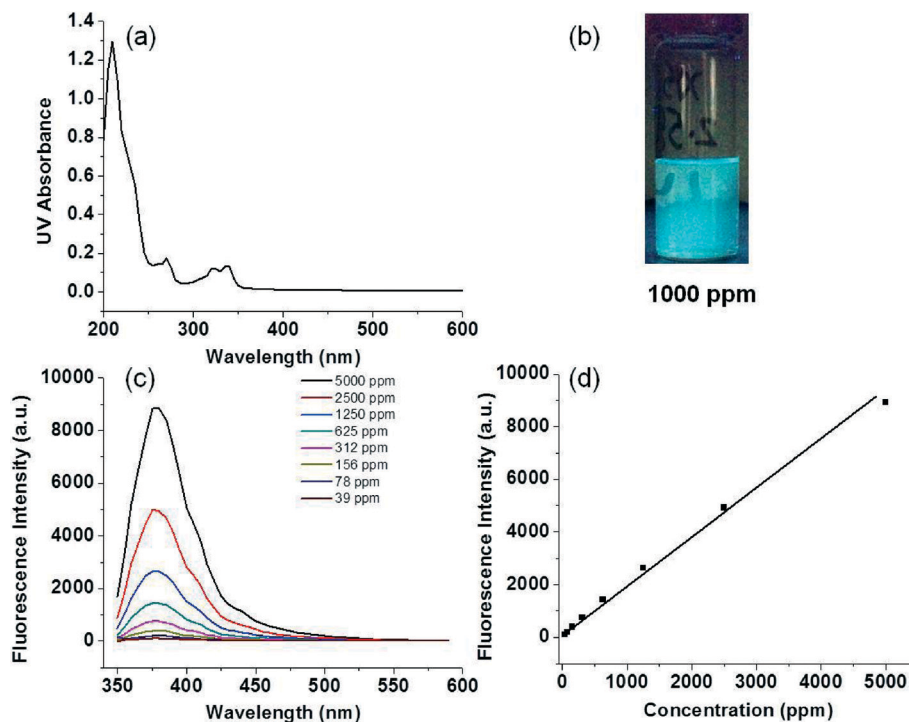


Fig. 9 (a) UV-vis spectrum of polymer functionalized SiO<sub>2</sub>-NPs; (b) SiO<sub>2</sub>-NPs solution under UV excitation; (c) fluorescence spectra of SiO<sub>2</sub>-NPs at a series of concentrations; (d) fluorescence calibration curve of SiO<sub>2</sub>-NPs. HFE was used in all spectroscopic analysis.

fluorescence intensity is only linear with NP concentration when concentration is lower than 400 ppm. This is probably because the Fe<sub>3</sub>O<sub>4</sub>-NPs have a strong background absorption which reduces the light energy for fluorophore excitation. While at low concentration, background absorption of Fe<sub>3</sub>O<sub>4</sub> is greatly reduced, thus the incident light is exclusively absorbed by fluorophore molecules.

The UV spectrum of SiO<sub>2</sub>-NPs in Fig. 9a also shows the characteristic  $\lambda_{\max}$  of 1-pyrenylmethyl methacrylate at 340 nm. However, the strong baseline absorption corresponding to the absorption of Fe<sub>3</sub>O<sub>4</sub> is missing for SiO<sub>2</sub>-NPs. Therefore, SiO<sub>2</sub>-NPs show uniformly fluorescent emission from the bottom to top as shown in Fig. 9b. In the case of Fe<sub>3</sub>O<sub>4</sub>-NPs, only the upper solution under excitation is fluorescent and the bottom solution still exhibits the brown characteristic color of Fe<sub>3</sub>O<sub>4</sub>-NPs. The absence of UV absorption as present in the Fe<sub>3</sub>O<sub>4</sub> core accordingly makes the fluorescence calibration curve (Fig. 9d) become linear in a wide range of concentrations. Interestingly, the fluorescence of SiO<sub>2</sub>-NPs is much lower than that of Fe<sub>3</sub>O<sub>4</sub>-NPs at the same concentration which is likely due to the much lower polymer grafting density for SiO<sub>2</sub>-NPs.

#### Dispersion of NPs in scCO<sub>2</sub>

The dispersion of two types of NPs was tested in CO<sub>2</sub> as shown in Fig. 10 in a high pressure chamber equipped with a glass window. Both iron oxide and silica NPs are insoluble in liquid CO<sub>2</sub> (Fig. 10a and a') as indicated by the cloudiness of the solutions that make the metal bar barely visible. As the

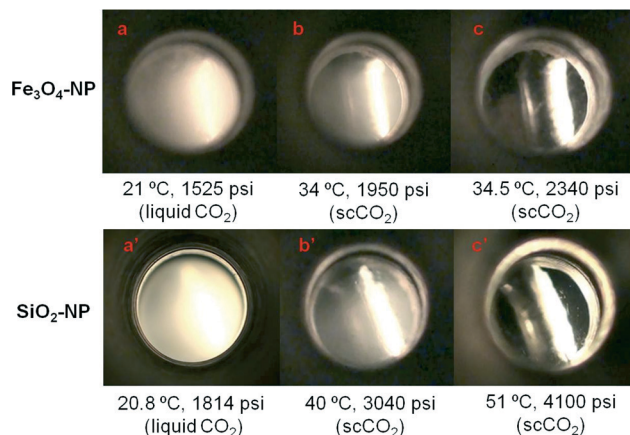


Fig. 10 Solubility tests of fluorinated polymer functionalized Fe<sub>3</sub>O<sub>4</sub>-NP and SiO<sub>2</sub>-NP in liquid CO<sub>2</sub> and scCO<sub>2</sub> under different CO<sub>2</sub> conditions. The solubility of the NPs is indicated by the transparency of the solution and the visibility of the metal bar inside the scCO<sub>2</sub> chamber.

temperature and pressure increased and the CO<sub>2</sub> entered the supercritical field, both NPs started to dissolve and the cloudiness gradual disappeared. The clear view of the metal bar (Fig. 10c and c') indicates the complete dissolution of NPs. The Fe<sub>3</sub>O<sub>4</sub>-NPs can be dispersed under milder conditions than SiO<sub>2</sub>-NPs. This difference in behavior is because of the higher grafting density of polymer on Fe<sub>3</sub>O<sub>4</sub>-NPs. More fluorinated polymer chains produce better solvation of the polymeric corona in scCO<sub>2</sub> which ultimately leads to dissolution at lower temperature and pressure conditions.

## Conclusions

Similar to previous work,<sup>24</sup> surface initiated ATRP was performed to graft a fluorinated polymer corona on the two types of inorganic oxide cores: Fe<sub>3</sub>O<sub>4</sub> and SiO<sub>2</sub>. These nanoparticles were less than 50 nm in diameter by DLS and electron microscopy. The nanoparticles can be well dispersed in scCO<sub>2</sub> or in hydrofluoroether, a scCO<sub>2</sub> analogue, without any observed aggregation. Copolymerization of the perfluorinated monomer with a small proportion of fluorescent monomer enables the soft corona to be highly fluorescent, providing an easy method of quantitative detection. Incorporation of fluorophore does not alter its good dispersion properties in scCO<sub>2</sub>. The NPs prepared here can, together with molecular chemical tracer, be used to assess rock fracturing for CO<sub>2</sub> sequestration.

## Acknowledgements

We acknowledge the Cornell KAUST Center for Sustainable Energy Development for financial support of Xu and Chen and for providing laboratory space and analytical instrumentation. We acknowledge the financial support of DOE (grant DE-FE0004633) and NSFC (21306049). We also acknowledge the Cornell Center for Materials Research (CCMR) for electron microscopy analysis.

## References

- 1 A. I. Cooper, *J. Mater. Chem.*, 2000, **10**, 207.
- 2 A. Busch and Y. Gensterblum, *Int. J. Coal Geol.*, 2011, **87**, 49.
- 3 A. H. Romang and J. J. Watkins, *Chem. Rev.*, 2009, **110**, 459.
- 4 A. O'Neil and J. J. Watkins, *MRS Bull.*, 2005, **30**, 967.
- 5 S. Holloway, *Energy (Oxford, U. K.)*, 2005, **30**, 2318.
- 6 R. Juanes, E. J. Spiteri, F. M. Orr and M. J. Blunt, *Water Resour. Res.*, 2006, **42**, W12418.
- 7 S. K. Subramanian, Y. Li and L. M. Cathles, *Water Resour. Res.*, 2013, **49**, 29.
- 8 J. F. McCarthy and L. D. McKay, *Vadose Zone J.*, 2004, **3**, 326.
- 9 J. M. DeSimone, Z. Guan and C. S. Elsbernd, *Science*, 1992, **257**, 945.
- 10 J. M. Desimone, E. E. Maury, Y. Z. Menciloglu, J. B. McClain, T. J. Romack and J. R. Combes, *Science*, 1994, **265**, 356.
- 11 A. I. Cooper, J. D. Londono, G. Wignall, J. B. McClain, E. T. Samulski, J. S. Lin, A. Dobrynin, M. Rubinstein, A. L. C. Burke, J. M. J. Frechet and J. M. DeSimone, *Nature*, 1997, **389**, 368.
- 12 B. Grignard, C. Calberg, C. Jerome, W. Wang, S. Howdle and C. Detrembleur, *Chem. Commun.*, 2008, 5803.
- 13 W. Senaratne, L. Andruzzi and C. K. Ober, *Biomacromolecules*, 2005, **6**, 2427.
- 14 L. K. Yeung, C. T. Lee Jr, K. P. Johnston and R. M. Crooks, *Chem. Commun.*, 2001, 2290.
- 15 L. Andruzzi, W. Senaratne, A. Hexemer, E. D. Sheets, B. Ilic, E. J. Kramer, B. Baird and C. K. Ober, *Langmuir*, 2005, **21**, 2495.
- 16 M. Y. Paik, Y. Xu, A. Rastogi, M. Tanaka, Y. Yi and C. K. Ober, *Nano Lett.*, 2010, **10**, 3873.
- 17 P. Meric, K. M. K. Yu and S. C. Tsang, *Langmuir*, 2004, **20**, 8537.
- 18 M. Sarkari, I. Darrat and B. L. Knutson, *Biotechnol. Prog.*, 2003, **19**, 448.
- 19 Y. Sun, X. Ding, Z. Zheng, X. Cheng, X. Hu and Y. Peng, *Eur. Polym. J.*, 2007, **43**, 762.
- 20 J. E. Martin, J. P. Wilcoxon, D. Schaefer and J. Odinek, *Phys. Rev. A*, 1990, **41**, 4379.
- 21 J. Liu, W. He, L. Zhang, Z. Zhang, J. Zhu, L. Yuan, H. Chen, Z. Cheng and X. Zhu, *Langmuir*, 2011, **27**, 12684.
- 22 M. C. McLeod, R. S. McHenry, E. J. Beckman and C. B. Roberts, *J. Phys. Chem. B*, 2003, **107**, 2693.
- 23 L. Wang, J. Luo, Q. Fan, M. Suzuki, I. S. Suzuki, M. H. Engelhard, Y. Lin, N. Kim, J. Q. Wang and C.-J. Zhong, *J. Phys. Chem. B*, 2005, **109**, 21593.
- 24 A. C. C. Chang, S. S. C. Chuang, M. Gray and Y. Soong, *Energy Fuels*, 2003, **17**, 468.